Research Article

Francesco Centracchio*, Lorenzo Burghignoli, and Umberto Iemma

Multiobjective optimisation of flight paths for noise level mitigation and sound quality improvement

https://doi.org/10.1515/noise-2021-0022
Received Dec 30, 2020; accepted Jul 07, 2021

Abstract: The present work deals with the multiobjective, multidisciplinary optimisation of takeoff and approach operations of a commercial aircraft aimed at the mitigation of the impact of aviation noise on the population. The innovative approach used here couples the minimisation of the aircraft noise level at the certification points with the improvement of the sound quality. The latter objective represents the main novelty of the present work and is addressed using a spectral–matching approach to make the aircraft noise as close as possible to a target sound. The rationale underlying the research is the development of a community–oriented approach to the assessment airport operations in view of the complete redefinition of the future airport scenarios. Indeed, the air traffic growth, the rapid expansion of urban areas around airports, and the expected advent of urban air mobility, are transforming the aviation noise into a serious hazard to the sustainable development of society. The sound–quality–based objective imposes a comprehensive multidisciplinary approach also in the procedural optimisation, due to the detail required to estimate the noise spectrum composition. Two merit factors are minimised, specifically the EPNL at the noise certification points and the L^p–norm of the difference between the noise produced by the configuration under analysis and a target sound. The target sounds are obtained by using sound engineering techniques aimed at the sound quality improvement, on the basis of the results of the psychometric tests campaigns performed within the projects SEFA and COSMA. The minimisation is achieved adopting a global evolution method, and the results are presented in terms of approximated Pareto frontiers for a single–aisle aircraft in both takeoff and landing conditions.

Keywords: Multidisciplinary Optimisation, Multiobjective Optimisation, Community Noise, Sound Quality, Noise Level, Trajectory Optimisation, Civil Aviation

1 Introduction

The rapid expansion of urban areas close to the airport facilities and the increase in air traffic in terms of daily movements are making the community noise problem a crucial aspect in the context of civil aviation sustainable development. Indeed, it is well known that aircraft noise causes adverse effects on life the quality and health of the residential community in the vicinity of airports. Consequently, the European Community has sponsored several scientific projects over the last twenty years to develop disruptive aircraft technologies, operational procedures with low chemical and acoustic environmental impact, and new air traffic management techniques. The work presented in this paper is the evolution in a multiobjective context of the achievements of the projects SEFA (Sound Engineering For Aircraft, FP6, 2004–2007 [1]) and COSMA (Community Noise Solutions to Minimise aircraft noise Annoyance, FP7, 2009–2012 [2]), and is developed within the framework of the ANIMA project (Aviation Noise Impact Management through Novel Approaches, H2020, 2017–ongoing [3]).

The purpose of the SEFA project [1] was to investigate sound quality requirements to combine with the classic noise level constraints within the aircraft design process in the conceptual design phase. Within that framework, the first attempt to consider the noise annoyance as an additional design constraint was developed. The concept of

***Corresponding Author: Francesco Centracchio:** Dipartimento di Ingegneria, Università Roma Tre, E-mail: francesco.centracchio@uniroma3.it
Lorenzo Burghignoli: Dipartimento di Ingegneria, Università Roma Tre, E-mail: lorenzo.burghignoli@uniroma3.it
Umberto Iemma: Dipartimento di Ingegneria, Università Roma Tre, E-mail: umberto.iemma@uniroma3.it

sound quality was exploited by a team comprising aircraft designers and manufacturers, psychoacoustics experts, and sound engineers to formalise an innovative though reliable design paradigm. The target sounds developed in SEFA, resulting from psychometric tests campaigns, are characterised by a high level of acceptance by the subjects of the tests. Such sounds are chosen among several synthesised aircraft sounds, normalised to the same EPNL (Effective Perceived Noise Level), focusing on the sound quality rather than the noise level. Specifically, a new acoustic descriptor, aimed at the assessment of the acoustic *distance* between two sounds, has been proposed [4, 5, 6, 7]: the basic principle is to quantify, in the time–frequency domain, the difference between the actual spectrum and a *weakly annoying* target spectrum, the latter identified based on a campaign of psychometric tests and advanced synthesis techniques. Therefore, the goal of the optimisation process is to force the noise emission to match the reference *weakly annoying* target sound.

The concept of noise annoyance has been extended within the contest of the project COSMA [2], to identify a set of realistic low–noise airport scenarios [8, 9]. COSMA was conceived within the X–Noise Collaborative Network, a worldwide framework of institutions and experts devoted to the civil aviation noise reduction challenges. The purposes of the project were addressed using a multidisciplinary approach through the integration of different competencies pertaining to aeronautical engineering, sound engineering and psychoacoustics. Special attention has been paid to the definition of different *optimised airport scenarios*, which consist of variations with respect to a baseline reference scenario in terms of technological improvements and/or operational procedure. Each scenario allowed the deep investigation on the potential benefits related to specific improvements, in terms of aircraft design or change in flight paths, related to the annoyance. To this aim, several multiobjective optimisation campaigns have been performed [7, 6] to propose novel manoeuvres sequences for both departure and approach procedures, aimed at the simultaneous abatement of chemical and noise pollution as well as the noise annoyance.

The *scenario* paradigm has become one of the central pillars of the ANIMA project [3]. ANIMA aims to develop innovative methods and suitable tools to mitigate and manage the effects of aircraft noise and improve the quality of life near airports. The used approach is such to facilitate both the airport growth and the aviation industries competitiveness, in compliance with the severe environmental constraints. ANIMA consortium, as for COSMA, is composed of multidisciplinary excellence. Industries, SMEs, RTOs, universities, airports and local authorities from 11 countries join forces to establish a joint strategic research roadmap for the aviation noise reduction challenges.

In such a context, the present work is being pursued to extend the results obtained in SEFA and COSMA, satisfying the needs of the ANIMA project. The design of low–noise flight paths for both takeoff and landing procedures is assessed by including multiple noise descriptors. For instance, the possibility of estimating sound quality and levels in areas characterised by different requirements (*e.g.*, a residential area, a school, a business district or a hospital) and located in the broad area affected by the aircraft noise is explored. Although capable of handling an arbitrary number of objective functions to optimise, the analysis presented here aims at simultaneously minimising the noise level and improve the sound quality in two different areas. The results refer to the takeoff and the approach procedures of a single–aisle aircraft. Given the methodological approach of this work, the location of areas where the objectives are computed is here entirely arbitrary. The aircraft flight paths have been optimised and analysed within the in-house Multidisciplinary Conceptual Robust Design Optimisation (MCRDO) framework FRIDA, (Framework for Innovative Design in Aeronautics [4, 5, 7, 6, 10, 8, 11, 12, 13, 14, 15]). The two objectives to be minimised are the EPNL at the noise certification point, along with the L^p norm of the difference between the noise produced by the aircraft related to the flight path under analysis and the *weakly annoying* target sound. It is worth noting that L^p norms of different orders can be used to build objectives that focus to local and distributed differences. This property has a paramount relevance when comparing sounds, as low values of p enhance the contribution of broadband noise differences, whereas high values of p emphasise local tonal components differences. This property has been extensively investigated on benchmark spectra [16] and can be effectively exploited when the effect of tonal components is explicitly available. The target sounds have been synthesised based on the psychometric tests campaigns performed in SEFA and COSMA projects. It should be emphasised that the direct integration of psychometric tests within a MDO framework is not practicable, unless a model of the human response is available. Preliminary activities aimed at this objective have been carried out in SEFA and COSMA, and are currently addressed in ANIMA. The constrained optimisation problem is solved by using the Particle Swarm Optimisation (PSO) method, a gradient–free global technique introduced by Kennedy and Russel [17], in an original deterministic implementation (DPSO) [18, 19]. Finally, the numerical results are presented in terms of approximated Pareto frontiers for both takeoff and landing conditions.

The paper is organised as follows. The formalisation of the optimisation problem is presented in Sec. 2, with details on the objective functions to be minimised and the formalisation of all the constraints. In Sec. 3, the numerical results are presented for takeoff and landing procedures, and the optimal solutions are described and discussed (in Sec. 3.1 and Sec. 3.2 respectively). Eventually, Sec. 4 gathers some concluding remarks. Appendix A provides details on the MCRDO framework FRIDA, used for the optimisation problems presented here, whereas in appendix B and appendix C are reported the computation methods for the objective functions under consideration.

2 The optimisation problem: noise level and sound quality

Aeroacoustics emissions strongly interplay with the flight path because of the source-receiver relative distance and the aircraft settings (in terms of aircraft velocity, engine rotational speed, high–lift devices and landing gear deployment, etc.). As deeply investigated [16], the tonal and broadband components related to the propulsion system (fan and compressor, turbine, buzz–saw, jet) depend on the engine settings (which is a function of the required thrust), thus on the trajectory mechanics. The airframe noise spectral characteristics are mainly linked with the aircraft speed and orientation and the high–lift devices deployment. Therefore, the change in trajectory completely redefine the aircraft parameters, and the acoustic emission in terms of level and spectral content constitute a complex function of such parameters. The purpose of the analyses presented in this work is the abatement of the noise level and the improvement in the sound quality in two different areas, for the takeoff and approach operations. This target is accomplished by minimising both a standard acoustic descriptor related to the acoustic level and the Sound–Matching index [6]. The analysed flight paths are modelled using a set of P points defined, with an appropriate time step, based on the definition of Q segments. The generic constrained multiobjective Optimisation Problems (MOP) is formalised as

$$\begin{aligned} \min/\max \left[J_k(\mathbf{x})\right], &\quad k = 1, \dots, K \text{ and } \mathbf{x} \in \mathcal{D} \\ \text{with bounds } x_n^L \le x_n \le x_n^U, &\quad n = 1, \dots, N \\ \text{subject to } g_i(\mathbf{x}) \le 0, &\quad i = 1, \dots, I \\ \text{and } h_j(\mathbf{x}) = 0, &\quad j = 1, \dots, J \end{aligned} \tag{1}$$

being $J_k(\mathbf{x})$ the k–th *objective function* wit.h $\mathbf{x}$ the vector containing the N *design variables* $x_n \in \left[x_n^L, x_n^U\right]$ (or, equivalently, $\mathbf{x} \in \mathcal{D}$), $g_i(\mathbf{x})$ the *inequality constraints* and $h_j(\mathbf{x})$ the *equality constraints*. The *feasible set* consists in the set of $\mathbf{x}$ in the design space $\mathcal{D}$ which satisfies the given constraints. The MOP solution consists of a set of solutions such that it is possible to improve further one of the objectives solely at the expense of at least another one. Such solutions are called *non–dominated* and constitute the Pareto frontier.

The proposed multiobjective approach is meant to enrich a classic noise-level-mitigation approach. The minimisation of the noise level is demonstrated to lead the most significant benefit to the airport community. Noise quality improvement cannot substitute the effort in reducing the noise level, and the use of a MO approach guarantees the identification of all the solutions that can potentially satisfy the trade–off and provide the designer with the broadest range of choices. In addition, the presented multiobjective approach can be further extended to include additional objectives related to chemical emissions and air quality, in compliance to the current trends in the research for sustainable aviation.

The acoustic descriptor used here for the level minimisation is the EPNL (Effective Perceived Noise Level): according to the ICAO standards, the EPNL is an evaluator of the subjective effects of aircraft noise on the community. It consists of the instantaneous perceived noise level PNL (Perceived Noise Level) corrected for spectral irregularities and duration. In the present work,

$$J_1(\mathbf{x}) = \text{EPNL} \tag{2}$$

evaluated at the certification points (see appendix B for details).

The improvement in sound quality deserves a more detailed discussion. Such a concept is a recent approach to the noise–oriented optimisation analysis in aeronautics [4, 5], developed within the EU–funded research projects SEFA (Sound Engineering For Aircraft, FP6/2004–2007) and its follow–up COSMA (Community Oriented Solutions to Minimize aircraft noise Annoyance, FP7/2009-2012), where the sound quality has been used as a multi–level optimisation constraint [7, 6]. Basically, the sound quality improvement consists in the estimation of the matching between the noise generated by the aircraft actual configuration and a target sound, synthesised as a result of psychometric tests aimed at the identification of a *weakly annoying* sound. The objective function $J_2(\mathbf{x})$ is thus a suitable index

$$J_2(\mathbf{x}) = \mathcal{I}_{SM} \tag{3}$$

representative of the *distance* in the vector space of all the possible spectra, between the noise emission of the analysed configuration and the target sound: it is defined as

the L^2 norm of the difference between the spectra, and the calculation procedure is presented in [6] and reported in Appendix appendix C. It should be noted that $\mathcal{I}_{SM}$ constitutes one of the possible strategies to include the spectral characteristics of the noise within the optimisation processes and aims at defining a merit function linked to sound spectral characteristics. In this work, the target sounds (for both the takeoff and the approach phases) must be considered as a fixed input. The $\mathcal{I}_{SM}$ objective function is evaluated at a representative location in the middle of an urbanised area close to the airport boundary. The geographic verification of the chosen location shows how it can be representative of many European airports. Nonetheless, selecting the areas where the objectives are evaluated and the acoustic describer used for each area is arbitrary.

Suitable constraints must be imposed to ensure the realistic manoeuvre simulation. Specifically, the high–lift devices deployment (here assumed as a function of the aircraft speed) combined with the fuselage angle of attack must ensure, at the p-th trajectory sample, the vertical equilibrium preventing the stall (that occurs at α_{ST}). Accordingly, the constraint can be formalised as it follows

$$g_1(\mathbf{x}) = \sum_p \max\left(0, \frac{\alpha_p}{\alpha_{ST}} - 1\right) \tag{4}$$

Furthermore, the engine operating points must be such that N1 (the rotational velocity of the low–pressure spool) never exceeds the overspeed (subscript OS) for takeoff and never passes below the idle condition (subscript ID) in the approach operation, thus

$$\begin{aligned} g_2(\mathbf{x})|_T &= \sum_p \max\left(0, \frac{N1_p}{N1_{OS}} - 1\right) \\ g_2(\mathbf{x})|_A &= \sum_p \max\left(0, 1 - \frac{N1_p}{N1_{ID}}\right) \end{aligned} \tag{5}$$

where T and A point out the takeoff and the approach procedure, respectively. In addition, to account for the normal load factor n variations, the following constraints must be formalised

$$g_3(\mathbf{x}) = \sum_p \max\left(0, \frac{n_p}{n_L^+} - 1\right) \tag{6}$$

$$g_4(\mathbf{x}) = \sum_p \max\left(0, 1 - \frac{n_p}{n_L^-}\right) \tag{7}$$

with n_L^+ and n_L^- the positive and negative limit normal load factor, respectively, to avoid structural failures. The constraints described by the Eqs. (4) to (7) are imposed at each p-th sample of the trajectory, with P the total number of sampled points. Eventually, to account for the maximum absolute value of the q–th ramp angle, the following constraint has been introduced

$$g_5(\mathbf{x}) = \sum_q \max\left(0, \frac{|\gamma_q|}{\gamma_{MAX}} - 1\right) \tag{8}$$

and, to ensure the cabin comfort, the maximum change in slope $\Delta\gamma_{MAX}$ between two consecutive trajectory segments has been imposed as

$$g_6(\mathbf{x}) = \sum_q \max\left(0, \frac{|\gamma_q - \gamma_{n-1}|}{\Delta\gamma_{MAX}} - 1\right) \tag{9}$$

being $2 < q < Q$, with Q the total number of segments. It is worth noting that, instead of solving the original constrained problem, a pseudo–objective function has been used to account for the optimisation constraints described by Eqs. (4) to (9). The pseudo–objective $\hat{J}_k$ has been defined using an external quadratic penalty function as it follows

$$\hat{J}_k(\mathbf{x}) = J_k(\mathbf{x}) + \frac{1}{\varepsilon}\sum_i \max(0, g_i(\mathbf{x}))^2 \tag{10}$$

being ε the penalty coefficient. Such a strategy allows addressing the solution of the corresponding unconstrained minimisation problem.

3 Numerical results and discussion

The optimisations have been carried out within FRIDA (Framework for Innovative Design in Aeronautics, see appendix A), a framework developed at the Department of Engineering of the Roma Tre University by the Aircraft Design and Optimization group. The case studies consist of 2D flight paths for a single–aisle aircraft with characteristics reported in Table 1. Starting from the mission requirements,

Table 1: Main characteristics of the mid–range aircraft.

Number of seats	164
Cruise Mach number	0.78
Cruise altitude	42000 ft
Range	3250 nmi
Number of engines	2
Maximum thrust per engine	111.2 kN
Bypass ratio	6.5
Engine placement	under the wing

FRIDA builds the aircraft model and evaluates the aerodynamic coefficients, to provide the input data to the flight

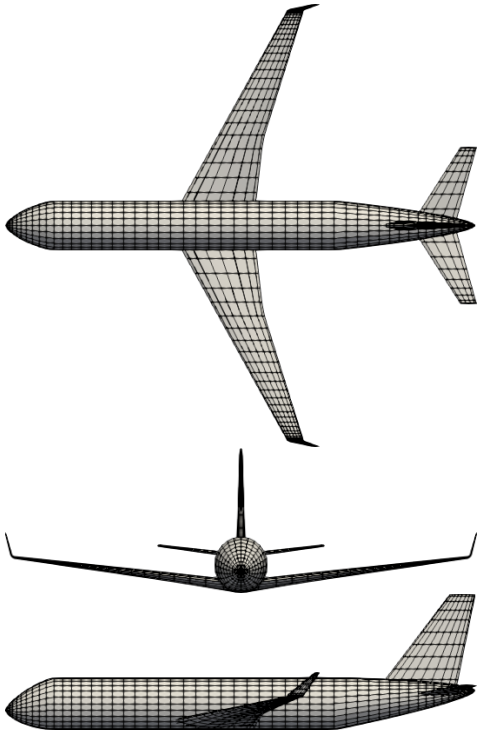

Figure 1: Top, front and side views of the single–aisle aircraft 3D model generated with FRIDA.

simulation module. A pictorial representation of the 3D aircraft model generated with FRIDA is in Figure 1.

The departure manoeuvre taken as reference is modelled on the ICAO procedures for the Airbus A320. The trajectory consists of 5 segments (6 input nodes), starting from the brake–release up to a distance of about 35.0 km from the runway. The geometric and the kinematic variables of the nodes are reported in Table 2.

Table 2: Reference takeoff procedure for the single aisle aircraft: geometric and kinematic variables.

node	x [m]	z [m]	v [m/s]
1	0.0	0.0	0.0
2	1698.6	0.0	83.7
3	4500.4	457.2	85.6
4	8648.7	914.4	87.5
5	15852.8	1179.4	136.2
6	35441.3	3048.0	149.7

The takeoff simulation has been carried out using an initial mass equal to the maximum takeoff weight (equal to 78 tons), keeping into account the weight loss due to the fuel consumption. Figure 2 shows the takeoff trajectory in terms of flight path profile and characteristic velocities.

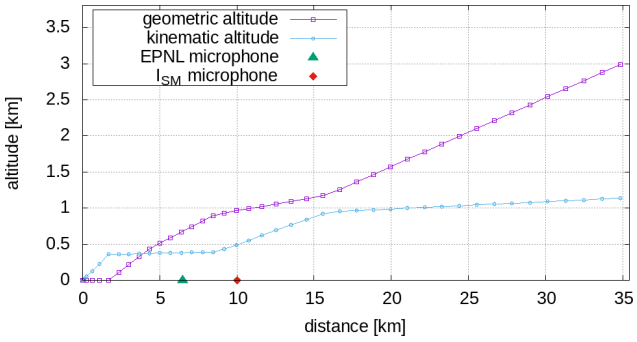

(a) Flight path profile

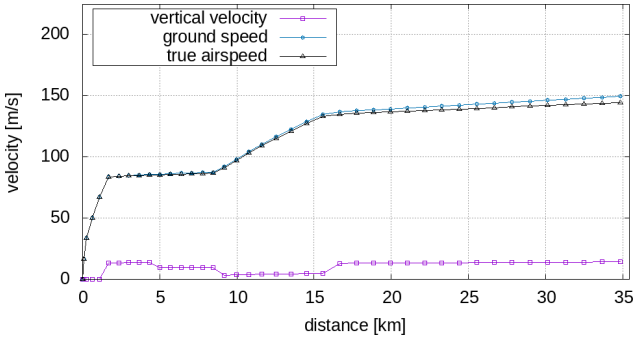

(b) Characteristic velocities

Figure 2: Reference takeoff procedure.

As shown in Figure 2a, the virtual microphone for the EPNL computation is that of the flyover reference noise measurement (located at 6.5 km from the point where the aircraft starts to roll), whereas the $\mathcal{I}_{SM}$ has been evaluated at 10.0 km from the start of the roll. A standard height of 1.2 m has been imposed for both the microphones. The target sound sonogram for used for the takeoff $\mathcal{I}_{SM}$ evaluation is in Figure 3.

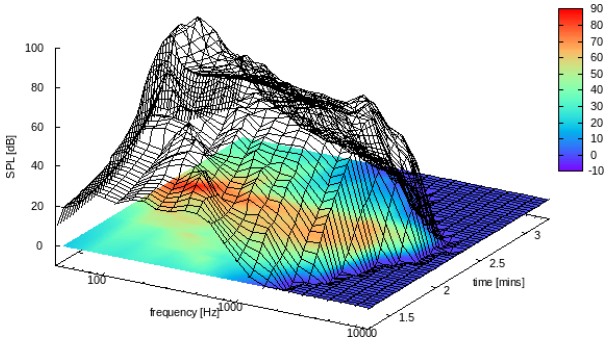

Figure 3: Takeoff target sound sonogram.

A summary of the aeroacoustic analysis results are reported in Table 3.

Table 3: Reference takeoff procedure: aeroacoustic analysis reslults.

mic.	x [km]	EPNL [EPNdB]	$\mathcal{I}_{SM}$
1	6.5	90.1	-
2	10.0	-	25.8

The reference approach trajectory is modelled on the standard procedure of the Airbus A320 landing manoeuvre. The trajectory consists of 6 segments (7 input nodes), starting at about 40.0 km from the airport and ending at the touchdown point on the runway. The geometric and the kinematic variables of the nodes are reported in Table 4.

Table 4: Reference approach procedure for the single aisle aircraft: geometric and kinematic variables.

node	x [m]	z [m]	v [m/s]
1	-39213.1	1828.8	140.6
2	-24262.8	914.4	134.4
3	-17447.8	914.4	98.0
4	-15202.8	796.7	92.9
5	-10297.6	539.7	70.0
6	0.0	0.0	68.2
7	925.1	0.0	15.4

The approach simulation has been carried out using an initial mass of about 60 tons, and the weight loss due to the fuel consumption is taken into account. Figure 4 shows the takeoff trajectory in terms of flight path profile and characteristic velocities.

The EPNL has been calculated at the approach reference noise measurement point (the microphone corresponds to a location 120 m below a -3° flight path originated from a point 300 m beyond the runway threshold), and the $\mathcal{I}_{SM}$ has been evaluated at 15.0 km from the touch–down point, as depicted in Figure 4a. The microphone height has been set equal to 1.2 m for both the virtual observers. The sonogram of the target sound used for the approach $\mathcal{I}_{SM}$ calculation is in Figure 5.

The aeroacoustic analysis for the approach procedure provides the results reported in Table 5.

The optimisation problem has been solved within FRIDA (for details see appendix A) using the Deterministic Particle Swarm Optimisation (DPSO) algorithm, an

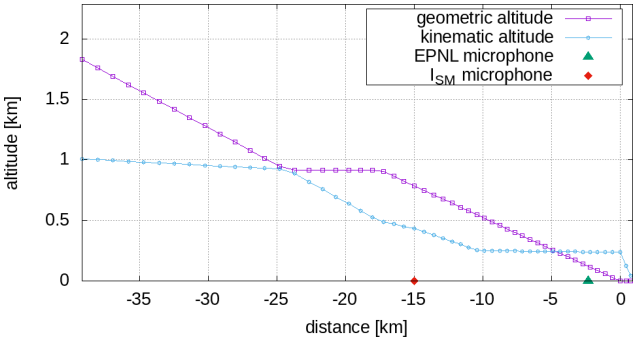

(a) Flight path profile

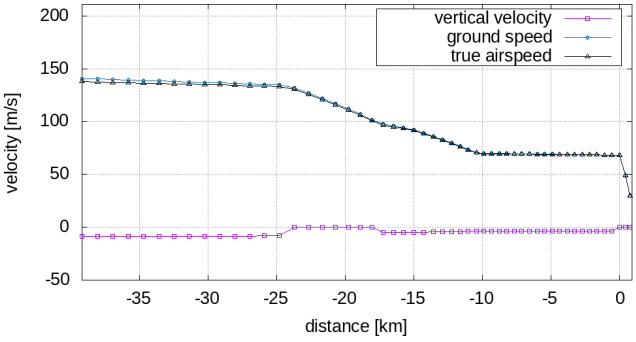

(b) Characteristic velocities

Figure 4: Reference approach procedure.

Table 5: Reference approach procedure for the single aisle aircraft: aeroacoustic analysis reslults.

mic.	x [km]	EPNL [EPNdB]	$\mathcal{I}_{SM}$
1	-2.3	100.9	-
2	-15.0	-	26.9

original deterministic implementation of the PSO (Particle Swarm Optimisation) method. A fixed–budget optimisation approach has been adopted, using 90 particles and 1000 iterations. The results are reported in terms of approximated Pareto frontiers, and three solutions will be analysed and compared: the solutions related to the minimum of each objective and the designer's choice, selected based on a ranking of the non–dominated solutions.

3.1 Takeoff phase

The optimisation process is aimed at finding the optimal path in terms of spatial and kinematic variables of the third, the fourth and the fifth trajectory node (see Table 2): the design variables are reported in Table 6 with the upper and lower bounds.

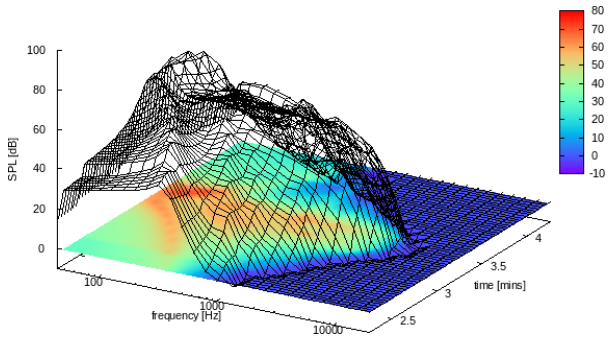

Figure 5: Approach target sound sonogram.

Table 6: Takeoff procedure optimisation variables: reference values with upper and lower bounds.

Variable	Lower boud	Reference	Upper bound
x_3 [m]	4000.0	4500.4	5000.0
z_3 [m]	400.0	457.2	500.0
v_3 [m/s]	85.0	85.6	86.0
x_4 [m]	7000.0	8648.7	10000.0
z_4 [m]	800.0	914.4	1000.0
v_4 [m/s]	87.5	87.5	110.0
x_5 [m]	13000.0	15852.8	17000.0
z_5 [m]	1000.0	1179.4	1300.0
v_5 [m/s]	110.0	136.2	140.0

The DPSO solutions distribution is shown in Figure 6 for the takeoff flight path, with the points related to the reference trajectory and the non–dominated solutions.

Figure 6 shows that the DPSO algorithm found a set of non–dominated solutions that considerably improves the values of the objective functions related to the reference flight path: the EPNL values related to the non–dominated solutions range from 86.5 to 87.5 EPNdB, whereas the $\mathcal{I}_{SM}$ from 22.7 to 26.6. The EPNL optimal solution has to a variation of about 4% in terms of EPNdB with respect to the reference solution, and a reduction of 12.4% can be observed for the solution related to the best $\mathcal{I}_{SM}$. A valuable strategy to the final choice is to rank the Pareto solutions by means of an additional objective. In this study, it has been decided to account for the amount of fuel W_f burnt during the simulated procedure to ensure minimal chemical emissions. Figure 7 depicts the mapped non–dominated solutions with the fuel burnt as a parameter.

The fuel burnt values are bounded by 660 kg and 700 kg, and the distribution is quite regular: notwithstanding, the W_f function minimum is related neither to the first nor to the second objective function, as shown in Figure 7. Such a ranking successfully drives the designer to the selection

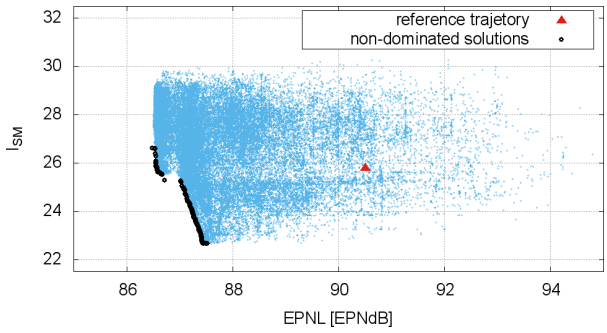

Figure 6: Takeoff trajectory: DPSO solutions, reference manoeuvre and non–dominated solutions.

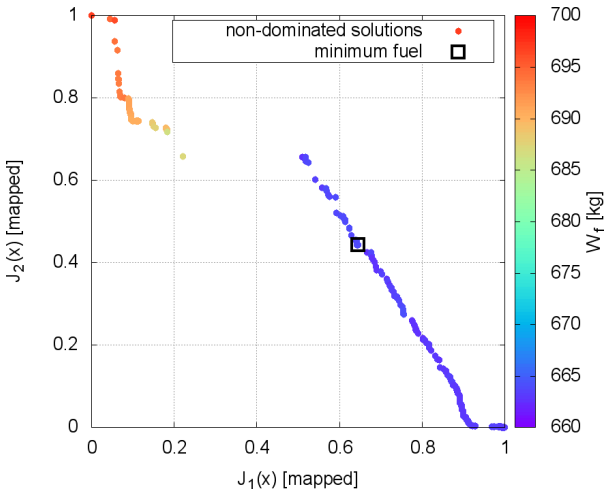

Figure 7: Takeoff trajectory: mapped non–dominated solutions and minimum fuel solution.

of the optimal flight path. Table 7 summarises the objectives for the analysed optimal takeoff trajectories.

Table 7: Takeoff optimal solutions.

Solution	EPNL	$\mathcal{I}_{SM}$	W_f
min[EPNL]	86.5 EPNdB	26.6	700.0 kg
min[$\mathcal{I}_{SM}$]	87.5 EPNdB	22.6	663.0 kg
min[W_f]]	87.2 EPNdB	24.4	660.0 kg

The comparison between the optimal takeoff trajectories, in terms of geometric altitude and ground speed is presented in Figure 8.

The analysis of Figure 8 shows that the solutions relative to the minimum of $\mathcal{I}_{SM}$ and to the minimum of W_f are quite similar in terms of the mechanics of the trajectory: such solutions could be nearby points in the co–domain. Figure 8b shows that the minimum EPNL trajectory exhibits an almost linear speed variation, thus a constant accelera-

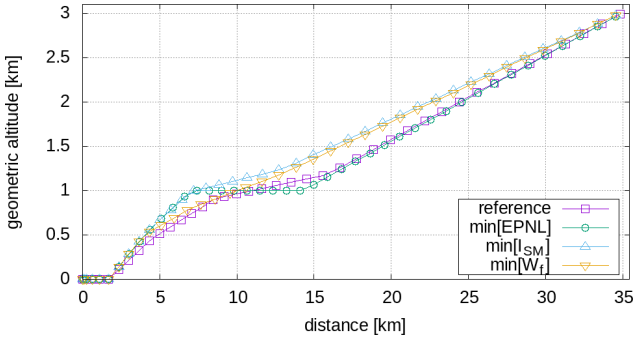

(a) Geometric altitude

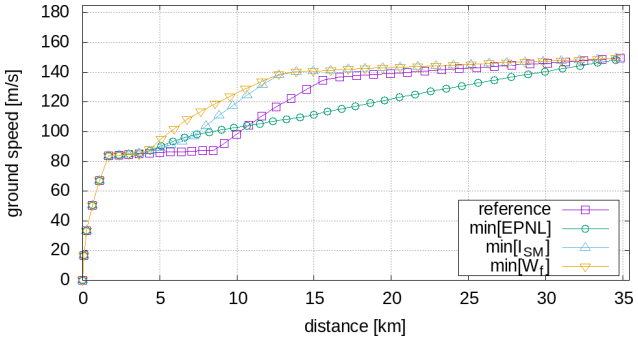

(b) Ground speed

Figure 8: Comparison between the optimal takeoff procedures: kinematic variables.

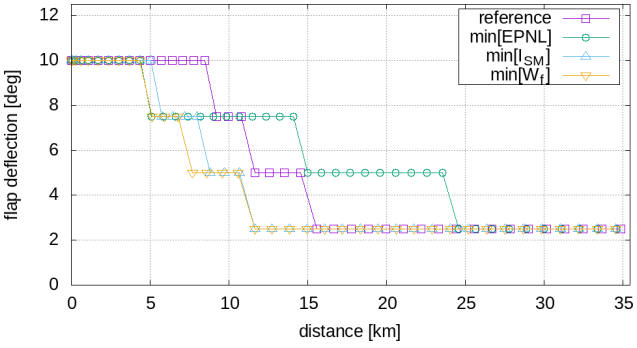

(a) Flap deflection

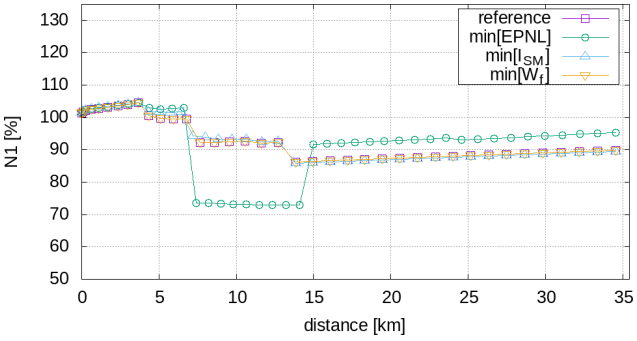

(b) N1

Figure 9: Comparison between the optimal takeoff procedures: procedural variables.

tion. In addition, it must be noted that the ramp angle above the $\mathcal{I}_{SM}$ virtual microphone of the optimal EPNL solution is the lowest if compared with the other paths: therefore, a better matching sound matching seems to be provided by higher distances from the observer, where high frequency components are more attenuated by the atmosphere. Figure 9 shows the comparison between the optimal takeoff trajectories in terms of procedural variables.

The minimum EPNL solution, as shown in Figure 9a, presents a substantial reduction of N1 in the region between 7 and 15 kilometres: this behaviour may be due to the need to minimise the noise generated by the engine jet. It is also interesting to note that, as depicted in Figure 9b, the minimum W_f solution seems to be driven by the flap deflection, meaning that the early removal of the high–lift devices is beneficial in terms of fuel burnt.

Considering what has been said, the designer choice falls on the solution corresponding to the minimum of W_f: such solutions corresponds to a 5.4% reduction of $\mathcal{I}_{SM}$ and 3.2% in terms of EPNdB with respect to the reference solution. In so doing, the optimality of the solutions belonging to the approximated Pareto front, as well as the ranking of the non–dominated solutions, have been both exploited.

3.2 Approach phase

The optimisation problem involves the spatial and kinematic variables of the second, the third and the fourth flight path node (see Table 4): the optimisation variables, with the upper and lower bounds, are reported in Table 8.

Figure 10 depicts the DPSO solutions distribution for the approach trajectory, the point related to the reference flight path and the non–dominated solutions.

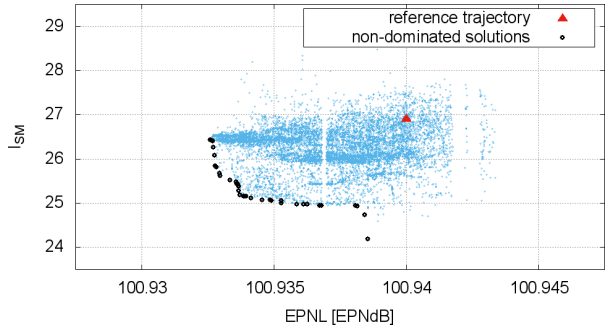

Figure 10: Approach trajectory: DPSO solutions, reference manoeuvre and non–dominated solutions.

Table 8: Approach procedure optimisation variables: reference values with upper and lower bounds.

Variable	Lower boud	Reference	Upper bound
x_2 [m]	-27500.0	-24262.8	-22500.0
z_2 [m]	914.4	914.4	1100.0
v_2 [m/s]	115.0	134.4	140.6
x_3 [m]	-19000.0	-17447.8	-16500.0
z_3 [m]	850.0	914.4	914.4
v_3 [m/s]	95.0	98.0	115.0
x_4 [m]	-15500.0	-15202.8	-13000.0
z_4 [m]	600.0	796.7	850.0
v_4 [m/s]	75.0	539.7	95.0

It is worth noting that, as highlighted by Figure 10, the EPNL values are almost equal to that of the reference case: this is due to the EPNL microphone location, below the last descent phase of the trajectory, that is assumed fixed at $-3°$ by the regulations. Indeed, different points of the design space just correspond to different values of $\mathcal{I}_{SM}$. Specifically, a $\mathcal{I}_{SM}$ reduction of 10% characterises the optimal $\mathcal{I}_{SM}$ solution and the one numerically related to the minimum EPNL also exhibits a reduction of about 1% if compared with the reference solution. It is interesting to note that all the solutions belonging to the Pareto frontier improve the initial flight path in terms of both analysed objectives. Table 9 summarises the objective functions for the analysed optimal takeoff trajectories.

Table 9: Approach optimal solutions.

Solution	EPNL	$\mathcal{I}_{SM}$
min[EPNL]	100.9 EPNdB	26.4
min[$\mathcal{I}_{SM}$]	100.9 EPNdB	24.2

Figure 11 shows the comparison between the optimal approach trajectories in terms of geometric altitude and ground speed.

The comparison between the optimal approach trajectories, in terms of procedural variables, is in Figure 12.

Since the same value of EPNL characterises all optimal solutions, the designer is allowed to select the solution corresponding to the minimum of $\mathcal{I}_{SM}$: this result is particularly important as it provides an additional degree of freedom within the optimisation of low-noise airport procedures. The optimal solution is characterised by a continuous descent path (see Figure 11a) with an almost constant variation of the ground speed up to -10 km, *i.e.* where the

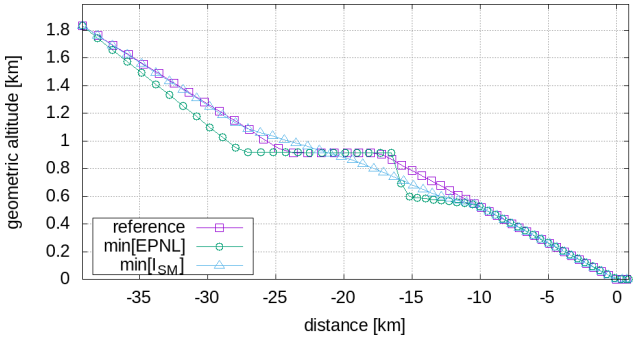

(a) Geometric altitude

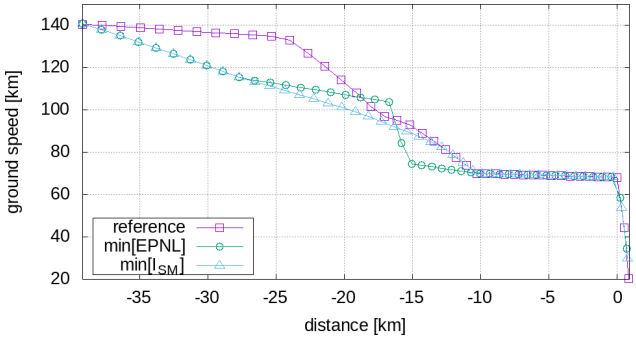

(b) Ground speed

Figure 11: Comparison between the optimal approach procedures: kinematic variables.

fixed segment starts. Furthermore, it is interesting to note in Figure 12a how the flap deflections are anticipated with respect to the reference trajectory, to preserve the vertical equilibrium at lower speed. Furthermore, since the variations of N1 with respect to the reference configuration (see Figure 12b) have no influence on the EPNL (because of the large distance from the EPNL virtual microphone), their only effect is to modify the spectral characteristics of the signal at the $\mathcal{I}_{SM}$ receiver.

4 Concluding remarks

The paper presents a multiobjective optimisation of takeoff and approach low–noise procedures of commercial aircraft. Accounting for the challenging environmental targets imposed by authorities, the feasibility of introducing alternative paradigms in the management of airport noise is becoming an imperative need. To simultaneously mitigate the aircraft noise level and improve the sound quality in terms of spectral content, two merit factors are minimised through a multiobjective and multidisciplinary optimisation problem. The first objective function is the Effective Perceived Noise Level at the noise certification points, whereas the index

> Centracchio F, Rossetti M, Iemma U. Approach to the Weight Estimation in the Conceptual Design of Hybrid-Electric-Powered Unconventional Regional Aircraft. Journal of Advanced Transportation. 2018;2018.
> Bernardini G, Centracchio F, Gennaretti M, Iemma U, Pasquali C, Poggi C, et al. Numerical Characterisation of the Aeroacoustic Signature of Propeller Arrays for Distributed Electric Propulsion. Appl Sci. 2020;10.
> Diez M, Iemma U. Multidisciplinary conceptual design optimization of aircraft using a sound-matching-based objective function. Engineering Optimization. 2012;44(5):591-612 Available from: https://doi.org/10.1080/0305215X.2011.591791.
> Kennedy J. Particle swarm optimization. In Proceedings of the 1995 IEEE International Conference on Neural Networks. 1995;4:1942-8.
> Campana E, Diez M, Fasano G, Peri D. Initial particles position for PSO, in Bound Constrained Optimization. Advances in Swarm Intelligence. 2013;(June).
> Pellegrini R, Serani A, Leotardi C, Iemma U, Campana EF, Diez M. Formulation and parameter selection of multi-objective deterministic particle swarm for simulation-based optimization. Applied Soft Computing. 2017;58:714731. Available from: http://www.sciencedirect.com/science/article/pii/S1568494617302661.
> Morino L. Boundary Integral Equations in Aerodynamics. Applied Mechanics Review. 1993;46(8):445-66.
> Morino L, Mastroddi F, De Troia R. Matrix fraction approach for finite state aerodynamic modeling. AIAA journal. 1995.
> Raymer D. Aircraft design: a conceptual approach; 1992.
> Fink MR. Approximate prediction of airframe noise. Journal of Aircraft. 1976;13(11):833-4.
> Fink MR Airframe noise prediction. FAA RD. 1977.
> Heidmann M. Interim prediction method for fan and compressor source noise. NASA CR 198300. 1975.
> Morfey C, Fisher M. Shock wave radiation from a supersonic ducted rotor. Aeronaut J. 1970.
> McAlpine A, Fisher M. On the prediction of buzz saw noise generated by an aero engine. 2000.
> Sutherland L, Piercy J. Method for calculating the absorption of sound by the atmosphere. In: 88th Meeting of the Acoustical Society of America; 1974.
> Burghignoli L, Centracchio F, Iemma U, Rossetti M. Multi-objective optimization of a BW aircraft for noise impact abatement. In: 25th International Congress on Sound and Vibration, ICSV25, Hiroshima, Japan; 2018.
> Iemma U, Pisi Vitagliano F, Centracchio F. Life Cycle Costs and Infrastructural Investments Induced by Unconventional Low-Noise Aircraft. In: InterNoise 2015 Proceedings, San Francisco; 2015.
> (ICAO) ICAO. Annex 16 - Appendix 2, Environmental Protection.

A The MCDO Framework FRIDA

The Multidisciplinary Conceptual Robust Design Optimisation (MCRDO) framework FRIDA (Framework for Innovative Design in Aeronautics) has been used for the analyses presented in this work. FRIDA can deeply describe the aircraft from a multidisciplinary viewpoint, and it turns out to be suitable for all the applications that require the aircraft configuration definition, the environmental impact estimation (taking into account both the acoustical and chemical emissions) combined with financial metrics. It is worth noting that the algorithms used for the aircraft analysis are, whenever possible, prime-principle based, as FRIDA has been developed also to assess the conceptual design of innovative aircraft [14, 15], for which the designer cannot rely on past experience or literature data.

The physical model used for the aerodynamic is that of a quasi-potential flow [20], i.e. the flow that can be considered potential everywhere except on the surface of the wake. The velocity-potential is then calculated using a boundary element method starting from an integral formulation based on the assumptions of incompressible flow and prescribed (and fixed) wake surface.

$$\varphi(\mathbf{x}, t) = \int_{S_B} G\chi \quad \varphi \frac{\partial G}{\partial n} \quad dS(\mathbf{y}) \int_{S_w} [\Delta\varphi_{TE}]^{\tau} \frac{\partial G}{\partial n} dS(\mathbf{y}) \tag{11}$$

The formulation is coupled with a boundary-layer integral model to account for the effects of viscosity providing an adequate estimation of the viscous drag, which is essential for the flight mechanics and performance analysis. The numerical solution of Eq. (11) is provided by a zeroth-order Boundary Element Method (BEM).

The structural analysis module of the wing is based on a 6-dof torsional-bending equivalent beam model with geometric and structural varying parameters along the three spatial directions. These include the geometrical dimensions of the structural elements, the taper of the wing, the characteristics of mass and both the bending and torsional moments of inertia. A linear variation law is used for the geometrical parameters of the wings and the tail. The structural problem is solved using a modal approach considering constant boundary conditions in the joint sections of the wings and tail surfaces with the fuselage. The approximate modes of vibration are calculated with a FEM model of the wing, by using the following representation for the displacements

$$\mathbf{u}(\mathbf{x}, t) = \sum_{m=1}^{M} q_m(t)\Phi_m(\mathbf{x}) \tag{12}$$

The numerical solution of Eq. (12) provides the diagonal matrix Ω of the wing natural frequencies. An accurate analysis of the masses distribution, including structures, payload, crew and operational items, allows the estimation of the centre of gravity $\mathbf{x}_{cg}$ of the actual aircraft configuration.

The estimation of both the flutter and the divergence speeds is also performed. The aeroelastic analysis is ob-

tained by the interaction between the aerodynamic variables, assumed constants, and the structural dynamics variables. A Reduced Order Model (ROM) is employed for the approximation of the matrix collecting the aerodynamic forces [21], to carry out an efficient aeroelastic analysis. Following this approach, the analysis can be reduced to the study of the roots locus, avoiding the use of more complex techniques, which could represent an excessive computational burden within the context of optimisation loop.

The flight mechanics is solved in order to ensure the static and dynamic balance of forces and moments. The static longitudinal stability, a fundamental requirement for the plane, is provided by imposing that the derivative of the pitching moment with respect to centre of gravity $\mathbf{x}_{cg}$ is less than zero:

$$C_{M_\alpha} < 0 \tag{13}$$

With the aim at simulating entire missions, suitable corrections are used to take into account the aerodynamic effects of high-lift devices (flaps and slats), air-brakes, and landing gears [22]: this considerably reduces the computational costs, as the aerodynamic analysis at each sample of the trajectory would be too time-consuming.

The analysis of entire mission requires the knowledge of the engine operating points at each trajectory sample. As a complete engine thermofluidynamical analysis would be too burdensome, a semiempirical turbofan model, based on the fundamental physics and some additional data available to the authors was developed. For a given flight condition, the model provides the percentage of throttle, knowing the engine characteristics, as it follows

$$t_{\%} = f(\mathbf{X}_{fm}, \mathbf{X}_{eng}) \tag{14}$$

being $\mathbf{X}_{fm}$ the representative vector of the flight mechanics variables (altitude, drag force, actual aircraft weight, acceleration of the aircraft, ecc.) and $\mathbf{X}_{eng}$ the vector of the propulsion system characteristics (number of engines, engine pitch, bypass ratio, maximum thrust per engine at sea level, ecc.). When the throttle is computed, is easy to evaluate the rotational speeds $N1$ and $N2$ of respectively low–pressure and high–pressure spools, knowing the overspeed and idle conditions in terms of revolutions per minute. For each operating point, the jets velocity is calculated through the momentum equation and their temperatures are estimated with the energy balance. Thereafter the amount of fuel consumed is also estimated, in order to update the current aircraft weight.

The aeroacoustics includes models for the estimation of both airframe and propulsion noise. The models for the estimation of airframe noise of lifting surfaces, tail, high–lift devices and landing gears is based on semiempirical functions according to the Fink's model [23, 24]. Such a model compute the noise in the *far-field* by the superposition of elementary sources, for which are known spectral and directivity characteristics. The propulsion noise estimation is based on Heidmann's model [25] for the fan a the compressor noise, on Morfey and Fisher model [26, 27] for the *buzz-saw* noise. The jet noise is evaluated by means of polynomial regressions of experimental data. For the calculation of the one-third octave band Sound Pressure Level (SPL), the algorithms also take into account the Doppler effect, the atmospheric absorption [28], and the ground reflection. By means of a suitable postprocessing, the Sound Exposure Level (SEL) and the Effective Perceived Noise Level (EPNL) are also estimated. FRIDA also includes an innovative sound quality assessment method, developed during the EC-funded projects SEFA (Sound Engineering For Aircraft, FP6, 2004–2007) and COSMA (Community Noise Solutions to Minimise aircraft noise Annoyance, FP7, 2009–2012) projects [4, 5, 7, 6]. More recently, suitable metamodels to account for the noise shielding effects of BWB (Blended Wing Body) configuration have been implemented [13, 29].

FRIDA also includes a financial module which allows the estimation of financial implications from an airline company perspective [30, 8, 12]. Positive cash flows (related to revenues) and negative cash flows (fuel and maintenance costs, and social costs related to noise pollution) are estimated and actualised in order to estimate the Net Present Value of the airliner.

B Effective Perceived Noise Level

According to ICAO Annex 16 Appendix 2 [31], the EPNL (Effective Perceived Noise Level) evaluation starts from the knowledge of the SPL spectra: sound pressure levels values from 50 Hz to 10kHz are converted in noy values $N(k)$, then converted in instantaneous perceived noise levels $PNL(k)$ as it follows

$$PNL(k) = 40 + \frac{10}{\log 2} \log N(k) \tag{15}$$

With the aim of accounting the human response to the spectra irregularities, a suitable tone correction factor $C(k)$ calculated and added to the k–th PNL value, deriving the time–dependent $PNLT(k)$ curve (a time–sampling of 0.5s is required by regulations): the maximum value of the $PNLT(k)$ time envelope, $PNLTM$ can be determined. Last step is the evaluation of the duration correction factor D, defined as

$$D = 10log\left(\frac{1}{T}\int_{t_1}^{t_2} 10^{\frac{PNLT}{10}}\,dt\right) - PNLTM \tag{16}$$

being $T = t_2 - t_1$ the time interval in which the $PNLT(k)$ values do not reach values lower than $PNLTM - 10$.

C Sound Matching Index

Considering two functions $g(\mathbf{x})$ and $h(\mathbf{x})$ defined onto the domain $\mathcal{D}$, and let define the norm of $f(\mathbf{x}) = g(\mathbf{x}) - h(\mathbf{x})$ in the space $L^p(\mathcal{D})$ as it follows

$$||f(\mathbf{x})||_p = \left[\int_{\mathcal{D}} |g(\mathbf{x}) - h(\mathbf{x})|^p \, d\mathcal{D}\right]^{\frac{1}{p}} \tag{17}$$

where, by definition

$$\lim_{p\to\infty} ||f(\mathbf{x})||_p = \max_{\mathbf{x}\in\mathcal{D}}\{g(\mathbf{x}) - h(\mathbf{x})\}. \tag{18}$$

Within the noise–oriented optimisation framework, with the aim at defining a suitable metric to account for the matching between the two discrete functions representing the sounds, Eq. (17) can be used. Indeed, the noise reaching a microphone representing the listener, during a specific flight operation, is characterised a spectrogram, which provides the amplitude of the acoustic event, in the time–frequency domain. With the aim at matching the actual simulated noise emission with the reference target sound [4, 5, 7, 6], let consider the vector space defined by the difference between the spectrogram S_c of the current flight path and the spectrogram S_t related to the target sound

$$\Delta = S_c(f, t) - S_t(f, t) \tag{19}$$

The norm of Δ in the L^p space can be used as a metric to be minimised to match the actual spectrogram with the target one. The sound-matching index $\mathcal{I}_{SM}$ can be formalised as it follows

$$\mathcal{I}^p_{SM} = ||\Delta||_p = \left[\frac{1}{T}\frac{1}{F}\int_{t_1}^{t_2}\int_{f_{min}}^{f_{max}} |S_c(f, t) - S_t(f, t)|^p \, df dt\right]^{\frac{1}{p}} \tag{20}$$

being $T = t_2 - t_1$ and $F = f_{max} - f_{min}$. The normalisation with respect to the domain measure of is not present in the standard definition of the L^p-norm, but does not modify the asymptotic behaviour of the norm, defined by Eq. (18). It is worth noting that $||\Delta||_1$ represents the volume bounded by the two spectrograms, whereas $||\Delta||_\infty$ corresponds to the maximum value of their point–wise difference in the time-frequency plane. In fact, low values of p enhance the contribution of distributed differences, whereas high values of p emphasise local differences. This property has a paramount relevance when comparing sounds, as low values of p enhance the contribution of broadband noise differences, whereas high values of p emphasise local tonal components differences.